TYPE: Regular Paper, **FIELD:** Biochemistry, **TOPIC:** Protein Structure

Structure of the *Acinetobacter baumannii* PmrA receiver domain and insights into clinical mutants affecting DNA-binding and promoting colistin resistance

Samantha Palethorpe[1], Morgan E. Milton[2], Everett C. Pesci[1], and John Cavanagh[2*]

[1]Department of Microbiology and Immunology

Brody School of Medicine

East Carolina University

Greenville, NC 27834

United States

[2]Department of Biochemistry and Molecular Biology

Brody School of Medicine

East Carolina University

Greenville, NC 27834

United States

***Corresponding author:** cavanaghj19@ecu.edu, +1 (252) 744-2684

RUNNING TITLE: *Acinetobacter baumannii* PmrA and structural insights

ABBREVIATIONS: Ara4N, 4-amino-4-deoxy-L-arabinose; BeF_3^-, Beryllium fluoride; EMSA, electrophoretic mobility shift assay; LPS, lipopolysaccharide; MIC, minimum inhibitory concentration; PDB, protein data bank; pEtN, phosphoethanolamine; SDS-PAGE, sodium dodecyl-sulfate polyacrylamide gel electrophoresis; wt, wild type.

ABSTRACT

Acinetobacter baumannii is an insidious emerging nosocomial pathogen that has developed resistance to all available antimicrobials, including the last resort antibiotic, colistin. Colistin resistance often occurs due to mutations in the PmrAB two component regulatory system. To better understand the regulatory mechanisms contributing to colistin resistance, we have biochemically characterized the *A. baumannii* PmrA response regulator. Initial DNA-binding analysis shows that *A. baumannii* PmrA bound to the *Klebsiella pneumoniae* PmrA box motif. This prompted analysis of the putative *A. baumannii* PmrAB regulon which indicated that the *A. baumannii* PmrA consensus box is 5′- HTTAAD N_5 HTTAAD. Additionally, we provide the first structural information for the *A. baumannii* PmrA N-terminal domain through X-ray crystallography, and we present a full-length model using molecular modeling. From these studies, we were able to infer the effects of two critical PmrA mutations, PmrA::I13M and PmrA::P102R, both of which confer increased colistin resistance. Based on these data, we suggest structural and dynamic reasons for how these mutations can affect PmrA function and hence encourage resistive traits. Understanding these mechanisms will aid in the development of new targeted antimicrobial therapies.

KEY WORDS

Acinetobacter baumannii, colistin resistance, PmrA, response regulator, two-component system.

Originally thought to be benign, the Gram-negative bacterium *Acinetobacter baumannii* is now a leading cause of hospital-acquired infections worldwide *(1,2)*. *A. baumannii* predominantly causes ventilator-associated pneumonia in addition to urinary tract infections, skin and soft tissue infections, meningitis, and bacteremia *(3,4)*. Outbreaks are often seen in intensive care units due to sustained colonization and resistance to environmental stresses. *A. baumannii* can survive for months on hospital surfaces and medical equipment, allowing easy, indirect patient to patient transmission *(5–8)*. In addition to such persistence, *A. baumannii* clinical isolates frequently display high levels of antibiotic resistance, with some studies estimating up to a 70% mortality rate due to multi-drug resistant infections *(9)*. From the standpoint of economic impact, the CDC reports that $281 million in healthcare costs are attributable to carbapenem-resistance *A. baumannii* infections alone *(10)*. Most alarmingly, there are reports of *A. baumannii* strains that are resistant to all available antibiotics *(11–13)*. With all this in mind, we are in dire need of novel antimicrobial strategies to tackle *A. baumannii*.

Colistin (polymyxin E) is a cationic polypeptide and is used as a last resort antibiotic due to its severe side effects, which include nephrotoxicity and neurotoxicity *(14)*. Colistin electrostatically interacts with the anionic lipid A component of lipopolysaccharide (LPS) in Gram-negative bacteria, causing permeabilization of the outer membrane. This disruption allows colistin to translocate across the outer membrane and destabilize the cytoplasmic membrane, resulting in cell death *(15)*. *A. baumannii* specifically has developed mechanisms to evade this last resort antibiotic; one study reports colistin resistance in 5.3% of *Acinetobacter* spp. clinical isolates found in the United States *(16)*. In general, colistin resistance often occurs due to changes in the outer envelope. These modifications reduce the overall negative charge of LPS, lowering colistin's affinity for the outer membrane *(17)*. Gram-negative bacteria achieve this by either addition of 4-amino-4-deoxy-L-arabinose (Ara4N) to the lipid A component of LPS, addition of phosphoethanolamine (pEtN) to lipid A, or by complete loss of LPS *(17–19)*.

Identification of the genes responsible for these mechanisms is vital for combating the rise in antimicrobial resistance.

Genetic mutations in the PmrAB two-component regulatory system are frequently identified in colistin-resistant *A. baumannii* strains *(14,18,20–24)*. The PmrAB two-component system has also been implicated in colistin resistance in other Gram-negative bacteria *(25)*, especially among the *Enterobacteriaceae* family members, including *Klebsiella pneumoniae, Escherichia coli,* and *Salmonella* spp. *(26–28)*. Most *pmr* mutations arise in patients receiving colistin treatment *(20,29)*. The *pmrCAB* operon encodes a pEtN transferase (PmrC), an OmpR/PhoB family response regulator (PmrA), and PmrA's cognate sensor kinase (PmrB).

The prototypical two-component system phosphorylation cascade triggers when a sensor kinase, such as PmrB, detects a change in the environment and autophosphorylates at a conserved histidine residue. The subsequent phosphotransfer to a conserved aspartate residue on the matching response regulator protein, PmrA, causes dimerization and activation of the response regulator. This leads to DNA binding and a change in transcription. This response to the initial stimulus allows bacteria to rapidly adapt to changes in the environment *(30,31)*. Thus, studying two-component systems is highly important to understand bacterial stress response mechanisms, especially among multidrug-resistant bacteria.

Recently, two PmrA mutations that significantly increased colistin resistance in *A. baumannii* were identified. The PmrA::I13M mutant strain conferred a 16–32-fold increase in colistin minimum inhibitory concentration (MIC), and the PmrA::P102R mutant strain conferred a 32-fold increase in colistin MIC *(24)*. Analysis showed that both strains had increased transcription of the *pmrCAB* operon compared to the parent strain. This led to the addition of pEtN to lipid A, resulting in increased colistin resistance. Since the PmrAB two-component system plays a vital role in *A. baumannii*, we wanted to explore the structural and biochemical impact of these PmrA mutations.

In this work, we first identified and characterized the previously unknown *A. baumannii* PmrA DNA-binding motif and began exploration of the PmrAB regulon. This then allowed us to study and compare the DNA-binding ability of wild type PmrA and a colistin-resistant mutant. Until this work, structural information for *A. baumannii* PmrA did not exist, so we elucidated the high-resolution structure of the PmrA N-terminal domain (which contains residues I13 and P102) using X-ray crystallography. Since full-length structures of response regulators are notoriously difficult to solve due to their flexible nature, we generated a computational homology model of full-length PmrA. Finally, using our structure and the full-length model, we investigated the PmrA::I13M and PmrA::P102R mutations to provide insight into how associated changes in structure and dynamics could promote DNA-binding, thereby leading to observed colistin resistance among *A. baumannii* clinical isolates. This work provides the initial structural groundwork for understanding the ramifications of the critical *A. baumannii* PmrA::I13M and PmrA::P102R mutants.

MATERIALS AND METHODS

Protein purification

Strains and plasmids used in this study are listed in Table S1. Full-length PmrA and the PmrA amino-terminal domain (PmrAN) from *A. baumannii* strain ATCC 19606 were expressed with an amino-terminal His_6 affinity tag using the expression vector pET28a (Novagen). pET28a-PmrA and pET28a-PmrAN were transformed into BL21 (DE3) *E. coli* cells. Overnight cultures were used to subculture into 2 L LB, that were then grown at 37°C, 160 rpm, to an optical density at 600 nm (OD_{600}) of 0.7. Cultures were then induced with 1 mM IPTG and shifted to 25°C, 120 rpm overnight. Cells were harvested and pellets were resuspended in 30 mL lysis buffer containing 25 mM Tris pH 7.9 and 500 mM NaCl. Cells were lysed by sonication, and the

resulting clarified supernatants were loaded onto an Ni-NTA agarose column (Qiagen) which had been equilibrated with lysis buffer. Next, the proteins were washed with 100 mL lysis buffer, followed by 100 mL 25 mM Tris pH 7.9 and 1 M NaCl. Proteins were eluted using an imidazole gradient (0-300 mM) in lysis buffer, and fractions were then dialyzed into 20 mM Tris pH 7.9, 400 mM NaCl, and 5 mM EDTA. The His_6 affinity tag was cleaved with the addition of 100 U thrombin for 2 h at room temperature and the reaction was quenched with 20 µM 4-(2-Aminoethyl)benzenesulfonyl fluoride hydrochloride (AEBSF) for 30 min at room temperature. Protein was concentrated using Millipore 10 K spin columns according to the manufacturer's protocol.

pET28a-PmrA::I13M was expressed and purified using the above protocol, except dialysis buffer contained 25 mM Tris pH 7.9 and 100 mM NaCl. Following cleavage and quenching as above, PmrA::I13M was loaded onto a Q Sepharose resin column, equilibrated with Q Sepharose buffer, as per the manufacturer's protocol (GE Healthcare). Protein was eluted using a NaCl gradient (0-500 mM) in 25 mM Tris pH 7.9, and concentrated using Millipore 10 K spin columns according to the manufacturer's protocol

Protein samples to be used for crystallography were further purified using a HiPrep™ 16/60 Sephacryl™ S-100 HR size exclusion column (Cytiva) equilibrated with 20 mM Tris pH 7.9 and 400 mM NaCl. Fractions containing purified protein (based on SDS-PAGE) were combined and concentrated using Millipore 10 K spin columns according to the manufacturer's protocol. Protein was stored at 4°C for crystallography experiments.

Chemical activation of proteins with beryllium fluoride

Samples were activated using beryllium fluoride (BeF_3^-) as previously described *(32–34)*. Briefly, 1 mg mL^{-1} purified protein was activated by addition of 7 mM $MgCl_2$, 5 mM $BeCl_2$, and 35 mM NaF. The solution was mixed and incubated at room temperature for at least 1 h.

X-ray crystallography

PmrAN was purified as described above. Crystals were grown at room temperature using hanging-drop vapor diffusion with a 1:1 ratio of protein to reservoir drop volumes. Hexagonal crystals were harvested from wells containing 0.2 M Lithium sulfate monohydrate, 0.1 M Bis-Tris pH 5.5, 25% w/v Polyethylene glycol 3350, and were flash-frozen in liquid nitrogen. X-ray diffraction data was collected using the APS beamline 23-ID-D (GM/CA) at a wavelength of 1.0332 Å. Data was indexed, merged and scaled using HKL-2000 *(35)* and molecular replacement was achieved using PHENIX Phaser-MR *(36)* with *Francisella tularensis* subsp. *novicida* BfpR as a search model (PDB ID 6ONT) *(37)*. The structure was refined in *Coot (38)* and using PHENIX.refine *(36)*. Structure figures were produced using PyMOL *(39)*.

Molecular modeling of full-length PmrA

A full-length model of PmrA was generated using MODELER v9.12 *(40)*. The model was constructed using the *A. baumannii* PmrAN crystal structure (PDB ID 7M0S) and homologs PhoP from *Mycobacterium tuberculosis* (PDB ID 3R0J) *(41)*, PmrA from *Klebsiella pneumoniae* (PDB IDs 4S04 and 4S05) *(42)*, KdpE from *E. coli* (PDB IDs 4KFC and 4KNY) *(43)*, BfmR from *A. baumannii* (PDB ID 5HM6) *(32)*, QseB from *F. novicida* (PDB ID 5UIC) *(44)*, and BfpR from *F. novicida* (PDB ID 6ONT) *(37)*. Five hundred models were generated from the sequence alignment of the above-mentioned protein structures with PmrA. Resulting models were scored based on the normalized DOPE (zDOPE) method *(40)*. The structure with the lowest zDOPE score was subsequently run through MolSoft ICM Full Model Builder version 3.8-7c to generate a fully refined model (MolSoft LLC). Finally, the model was run through PROCHECK and PSVS to evaluate the quality of the model *(45,46)*. The “best” model had the lowest zDOPE score, highest percentage of favored and allowed Ramachandran regions, and lowest MolProbity clash score. The model was further validated through comparison to the RoseTTAFold prediction of

the PmrA C-terminal domain *(47)*. The sequence of the DNA-binding domain was provided to the Robetta server (robetta.bakerlab.org). Output models were overlaid with the full-length model and RMSDs were calculated in PyMol *(39)*.

Simulations of point mutants

The prediction of changes in protein stability due to point mutations was carried out in ICM-Pro (MolSoft LLC). The full-length PmrA model was subjected to 10 rounds of biased probability Monte Carlo simulations using the Mutation - Protein Stability protocol outlined in the ICM User's Guide. The simulation uses flexible side chains for the specific mutated residue and neighboring residues while the rest of the structure remains rigid.

Electrophoretic mobility shift assays (EMSA)

DNA promoter fragments (Table S2) were designed based on the *K. pneumoniae* PmrA box (PDB ID 4S04) *(42)*, or using the *A. baumannii* ACICU genome *(48)*. Equimolar concentrations of single stranded DNA (Integrated DNA Technologies, Inc.) were annealed by heating at 95°C for 5 minutes in 20 mM Tris pH 7.9, 100 mM NaCl, 2 mM $MgCl_2$, and 1 mM DTT, followed by slow cooling to room temperature. Binding reactions containing 1 µM DNA and indicated concentrations of protein were incubated for 5 min at room temperature before loading onto pre-chilled 8% TBE-acrylamide native gels. Samples were electrophoresed at 80 V in 1x TBE running buffer and stained with ethidium bromide for 5 minutes before visualizing bands. Following this, gels were stained with Coomassie blue and imaged.

Fluorescent anisotropy DNA binding assay

A 25 bp oligonucleotide with a 5′-FAM (6-carboxyfluorescein) label was designed based on the *K. pneumoniae* PmrA box *(49,50)*. Equimolar concentrations of this KpPmrA_25mer_FAM-F single stranded DNA fragment and the complimentary KpPmrA_25mer-

R fragment (Table S2) (Integrated DNA Technologies, Inc.) were mixed and annealed by incubating on ice for 1 h. Serial dilutions of the indicated protein concentrations were added to wells of a black 96-well plate (BrandTech) containing 5′-FAM labeled dsDNA in 20 mM Tris pH 7.9, 100 mM NaCl, 2 mM $MgCl_2$, 0.1 mM DTT and 0.1 mg mL^{-1} BSA. The final reaction volume was 100 µL, and all assays were performed at room temperature. Fluorescent polarization was measured using a Synergy H1 Hybrid Multi-Mode microplate reader (BioTek) and Gen5 software (BioTek) at an excitation wavelength of 482 nm and an emission wavelength of 528 nm. To determine K_d values, data were analyzed using DynaFit software (BioKin Ltd.) to fit a standard equilibrium mechanism, a + b ←→ ab *(51)*. Each experimental assay was performed at least three times for each protein.

RESULTS AND DISCUSSION

A. baumannii PmrA binds to the *K. pneumoniae* PmrA box motif

The OmpR/PhoB family of response regulators controls transcription of numerous genes, including the *pmrCAB* operon, in response to a stimulus. It was originally shown that *A. baumannii* strains carrying PmrA::I13M and PmrA::P102R mutations had upregulated *pmrCAB* expression, that in turn led to increased colistin resistance *(24)*. Our hypothesis was that the DNA-binding affinity of the mutants compared to wild-type would be altered, resulting in the observed changes in *pmrCAB* transcription. To further expand on this finding, we wanted to compare the DNA-binding ability of wild-type (wt) PmrA and the mutants. To do this, we first needed to identify the *A. baumannii* DNA-binding motif.

Although the *A. baumannii* PmrAB regulon has not been fully identified, PmrA-regulated genes have been well defined in other Gram-negative bacteria, such as *Salmonella enterica* and *K. pneumoniae*. The majority of these gene products function in LPS production and

modification, and include pEtN transferases (*pmrC* and *cptA*), Ara4N biosynthesis genes (*pmrHFIJKLM* and *pmrE*), genes that alter the LPS core (*pmrG*), and genes that determine the LPS O-antigen chain length (*cld*) *(27,28,50)*. The PmrA DNA-binding motifs in these Gram-negative species appear to be homologous. The *S. enterica* PmrA recognition sequence consists of 5′-YTTAAK direct repeats *(27)* and the *K. pneumoniae* PmrA box consists of is 5′-CTTAAT and 5′-CCTAAG *(50)*. *S. enterica* PmrA and *K. pneumoniae* PmrA share 79.6% protein sequence identity, with 76.3% identity between their C-terminal DNA-binding domains *(52)*. It is therefore unsurprising that the two organisms have homologous DNA-binding motifs.

A. baumannii PmrA and *K. pneumoniae* PmrA share 39.6% sequence identity overall, with their C-terminal domains sharing 36.6% identity. However, the *A. baumannii* PmrA DNA-binding helix shares 54.5% sequence identity with the *K. pneumoniae* PmrA DNA-binding helix. Moreover, both helices contain four identical positively charged residues that potentially interact with DNA (*A. baumannii* PmrA residues H201, R204, K206, and K209) *(53)*. Due to this conservation, and the fact that *K. pneumoniae* PmrA and *S. enterica* PmrA share homologous DNA-binding motifs, we decided to test *A. baumannii* PmrA's ability to bind the *K. pneumoniae* PmrA box motif (KpPmrA_25mer, Fig. 1a). Electrophoretic mobility shift assays (EMSAs) showed that wt PmrA and PmrA::I13M bind to the KpPmrA_25mer (Fig. 1b). This suggests that the *A. baumannii* PmrA binding motif is similar to the *K. pneumoniae* PmrA box. We also generated a non-reversable activated construct of wt PmrA with the phosphomimic BeF_3^- (PmrA-BeF_3^-). This activation method has been shown to promote functional dimerization *(32–34)*. Dimerization is an important activation step as it often facilitates response regulator binding to tandem DNA motifs *(54)*. As expected, the EMSA showed that PmrA-BeF_3^- also binds to the KpPmrA_25mer (Fig. 1b). (All EMSA ethidium bromide-stained images and Coomassie Brilliant Blue-stained images have been overlaid in Fig. S1). While we would have liked to similarly study PmrA::P102R, regrettably, this mutant expressed mostly in the insoluble pellet fraction, so

no studies were possible. We are currently working to overcome this challenge. Unlike the full-length wt PmrA protein, the PmrA C-terminal domain alone was unable to bind to the KpPmrA_25mer (data not shown). This was somewhat expected since response regulators require communication between the N- and C-terminal domains via the flexible linker to coordinate structural and dynamic changes for DNA binding *(55,56)*. EMSA analysis of other response regulators, such as *A. baumannii* BfmR, also support this explanation *(32)*.

We next performed fluorescent anisotropy to determine the DNA-binding affinity of both wt PmrA and PmrA::I13M to KpPmrA_25mer with a 5′-FAM (6-carboxyfluorescein) label (KpPmrA_25mer_FAM). Wt PmrA binds to this DNA fragment with a 2-fold higher affinity (K_d = 8.5 ± 1.7 µM, Fig. 2a) than the PmrA::I13M mutated protein (K_d = 16.6 ± 2.3 µM, Fig. 2b). Next we tested wt PmrA and PmrA::I13M which had been activated using the phosphomimic BeF_3^- (Fig. 2c and 2d). As expected, the DNA-binding affinity of wt PmrA increased over 10-fold when activated with BeF_3^- (K_d = 0.78 ± 0.24 µM, Fig. 2c). Surprisingly, PmrA::I13M-BeF_3^- bound 55-fold tighter (K_d = 0.301 ± 0.088 µM, Fig. 2d) than inactive PmrA::I13M (Fig. 2b), and 2.5-fold higher than wt PmrA-BeF_3^- (Fig. 2c). These data suggest that the I13M mutation causes structural changes during activation that likely promote the dimerized conformation and therefore enhance DNA-binding. These DNA-binding assays give further support for the upregulation of *pmrCAB* transcription reported previously in PmrA mutants *(24)* with the assumption that PmrA binds to its own promoter.

The putative PmrAB regulon includes numerous genes required for LPS modifications

Several response regulators are capable of binding to their own promoters for autoactivation, including PmrA in *Salmonella* spp. *(27,57)*. Since PmrA mutations in *A. baumannii* are associated with increased *pmrCAB* transcription *(24)* we posited that *A. baumannii* PmrA also possesses autoregulatory activity. We analyzed the *pmrCAB* promoter region for motifs similar to the KpPmrA_25mer and identified a similar motif, 5′- TTTAAG N_5

TTTAAG, 48 bp upstream from the predicted translational start site of *pmrC* (Table I). Figure 3 shows that both wt PmrA and wt PmrA-BeF_3^- bind to this DNA fragment. This observation is indicative that PmrA is indeed autoregulatory and further confirms the *A. baumannii* DNA-binding motif.

We next analyzed promoter sequences from the putative *A. baumannii* PmrAB regulon. This regulon was originally suggested in a transcriptome study *(22)* that analyzed differentially expressed genes in clinical *A. baumannii* isolates that had accumulated mutations over the course of an infection. Clinical isolates containing mutations in the *pmr* operon shared 21 dysregulated genes, some of which, expectedly, have also been identified as colistin-responsive genes *(21,22)*. From this gene set, we identified 11 promoter regions that each contain homologous sequences to the KpPmrA_25mer sequence. Table I shows the motifs identified along with the predicted downstream gene functions.

As anticipated, half of the promoter regions identified in Table I regulate genes predicted to function in LPS biosynthesis and modification mechanisms. *pmrC,* ACICU_03001, and ACICU_01072 encode enzymes which modify lipid A and have all been associated with colistin resistance *(19)*. ACICU_02907 is also predicted to encode an enzyme involved in membrane phospholipid biosynthesis *(58)*. ACICU_02865 potentially encodes a mannosyltransferase, and ACICU_02867 belongs to the glycosyltransferase family 2, both of which may have a role in cell wall biosynthesis *(59)*. The remaining set of promoters are associated with various other gene functions, including biofilm adhesion (*pgaBCD*) *(60)*, or have not yet been characterized. Overall, these data clearly suggest that the PmrAB regulon is predominantly involved in production and maintenance of LPS. We propose that the *A. baumannii* PmrA consensus box is as follows: 5′- HTTAAD N_5 HTTAAD. We are currently pursuing this further to identify how each of these genes are regulated by PmrA.

Crystal structure of the *A. baumannii* PmrA N-terminal receiver domain

Our initial goal was to better understand the effects of mutations in the N-terminal receiver domain of PmrA (PmrAN). Since there was no structural information available on PmrAN, we solved the high-resolution structure of this domain through X-ray crystallography (Fig. 4). The protein crystallized in the $P12_11$ space group with unit cell parameters of a = 32.40 Å, b = 39.23 Å, and c = 91.27 Å, and α = γ = 90° and β = 95.66°. The structure was solved through molecular replacement using *F. novicida* BfpR (PDB ID 6ONT) *(37)* as a starting model and refined to 1.64 Å resolution with a crystallographic R_{work} of 0.1741 and R_{free} of 0.2136. Refinement corrected all Ramachandran outliers. Final statistics for data collection and refinement are listed in Table S3.

The PmrAN asymmetric unit contained two molecules representing a biologically relevant dimer in the active conformation (Fig. 4a). The dimeric state was confirmed through structural alignment with other known dimeric response regulator structures (Fig. S2). The final model (Fig. 4a) contains residues 1 – 224 (100%) of monomer A, and residues 1 – 223 (99.6%) of monomer B. As expected, each monomer follows the characteristic receiver domain α_5/β_5 fold, whereby five parallel β-sheets alternate with five amphiphilic α-helices, giving the final conserved β1-α1-β2-α2-β3-α3-β4-α4-β5-α5 conformation *(44,61–63)*. There were no structural discrepancies between the two monomers that interact via the α4-β5-α5 interface (Fig. 4). This specific interaction is highly conserved among OmpR/PhoB-type response regulators, providing a common dimerization mechanism *(32,37,61,64,65)*.

Although PmrAN was not activated with a phosphomimic prior to crystallization, we expected it to crystallize in a dimeric conformation based on previous receiver domain structures. It is generally accepted that phosphorylation of response regulators by their cognate sensor kinases stimulates dimerization and activation. However, within a crystal lattice, active conformations of response regulators are often observed in the absence of phosphorylation, leading to the more plausible hypothesis that the inactive and active conformations are in constant equilibrium *(55)*. A phosphorylation event simply shifts this balance to favor

dimerization *(66)*. The N-terminal domains of response regulators frequently crystalize in an active state, examples of which include *A. baumannii* BfmR (PDB ID H5M6), *E. coli* PhoP (PDB ID 2PKX) and *Staphylococcus aureus* ArlR (PDB ID 6IS1) *(32,64,67)*.

A notable structural feature of the PmrAN crystal structure is that R118 is captured in two alternative confirmations which share density between the two chains (Fig. 4b). R118 is located on the α5 helix and is conserved among the OmpR/PhoB family of response regulators. The typical orientation of R118, such as in PhoP (PDB ID 2PKX) *(68)* and ArlR (PDB ID 6IS1) *(67)*, allows H-bonding to the conserved D96 residue (located on the α4–β5 loop), that connects the two monomers at the dimer interface *(61)*. Alternatively, in our PmrAN structure, a second conformation of R118 H-bonds to a network of water molecules within the dimer interface.

To illustrate the structural conservation of response regulator receiver domains, we performed structural alignments of PmrAN against numerous other response regulators using PyMol (Fig. 5) *(39)*. These alignments have an average RMSD of 0.912 Å, indicating strong structural similarity between PmrAN and other OmpR/PhoB receiver domains (Fig. 5b).

Modeling of the *A. baumannii* full-length PmrA structure

The flexible nature of full-length response regulators that allows them to adopt multiple conformations often makes structural determination challenging. This was the case for full-length PmrA where, regrettably, all efforts to produce crystals that adequately diffracted were unsuccessful. To combat this, we have previously developed a hybrid method in which full-length structures are solved as separate N- and C-terminal domains. The individual domains are then spaced and oriented using distance restraints provided by chemical cross-linking and mass spectrometry *(32)*. With that in mind, we attempted to express and crystallize the C-terminal DNA-binding domain of *A. baumannii* PmrA (PmrAC), but we have been unsuccessful to this point.

In the meantime, we have generated a full-length model for *A. baumannii* PmrA (Fig. 6a) using our solved PmrAN structure (Fig. 4) and other OmpR/PhoB response regulator structures as homologs for the C-terminal domain. Overall, PmrA is predicted to bear significant structural homology to other OmpR/PhoB response regulators. To validate our model, we utilized RoseTTAFold to predict the structure of PmrAC *(47)*. RoseTTAFold is the latest advancement in protein structure prediction using deep learning to build computational models from protein sequences. Our full-length model is in close agreement with the RoseTTAFold results with an αC RMSD of 1.101 Å (Fig. 6b). This strongly suggests that we have built the best PmrA homolog possible with the currently available technology. The resulting model follows the archetypal OmpR/PhoB winged helix-turn-helix DNA-binding motif (Fig. 6a).

The full-length PmrA monomer model (Fig. 6a) consists of the N- and C-terminal domains joined by a twelve amino acid linker. As noted, the OmpR/PhoB family use this flexible linker region between the two domains to allow the protein to sample a range of conformations. The two most extreme conformations are described as “tucked” (N- and C-terminal domains proximal) and “extended” (N- and C-terminal domains distal), and play a role in correct binding of DNA *(42,43,56)*. Both conformations have been captured in the *K. pneumoniae* PmrA crystal structures (PDB IDs 4S04 and 4S05) *(42)*. In our *A. baumannii* model, PmrA is seen in the “tucked” state (Fig. 6a).

As expected, our full-length PmrA model displays the distinctive structural characteristics of the OmpR/PhoB family. Since response regulators have highly conserved structural motifs, we were curious how specific mutations such as I13M and P102R could cause potential perturbations leading to altered protein activity, such as DNA-binding ability (as demonstrated in Fig. 2 for PmrA::I13M) *(24)*. At this time, we have been unable to produce appropriate crystals of the mutants. With this in mind, we have generated homology models for comparative investigations.

The PmrA::I13M mutation likely alters the overall structure, plasticity, and intra-protein communication networks of PmrA to promote DNA binding

Although Sun *et al.* were the first to identify the novel PmrA::I13M mutation *(24)*, other studies have identified other mutations located around this position that confer colistin resistance (PmrA::M12I *(69,70)*, PmrA::A14V *(69)*). Both PmrA::M12I and PmrA::A14V mutations arose in *A. baumannii* strains isolated from patients undergoing colistin therapy *(69)*. PmrA::M12I was also identified as a spontaneous mutant on a colistin gradient plate *(70)*, and PmrA::I13M was isolated in a transposon mutant library after exposure to colistin *(24)*. These findings indicate that this region of PmrA is susceptible to advantageous mutations during exposure of *A. baumannii* to colistin.

The impact of the I13M mutation on the overall stability of PmrA was simulated using Molsoft ICM software (Molsoft LLC) (Fig. 7a). This program calculates the change in free energy of a mutant using the equation $\Delta\Delta G = \Delta G^{mutant} - \Delta G^{wild\ type}$, whereby $\Delta\Delta G > 0$ kcal/mol represents destabilization. We modeled the PmrA::I13M mutation in the N-terminal structure as a single domain, and also in the full length model. We then compared each mutant to their respective wild types. The data show that the I13M mutant has a $\Delta\Delta G$ value of 0.51 kcal/mol when compared to the PmrAN structure, and 0.31 kcal/mol when compared to the full-length PmrA model. Since both values are > 0 kcal/mol, the I13M mutation is predicted to cause structural instability whereby the protein becomes more amenable to conformational changes.

Both Ile and Met are non-polar, hydrophobic amino acids and are interchangeable via a single nucleotide mutation. However, unlike Ile, Met has unbranching side chains which, due to a low rotational barrier energy, offers increased flexibility *(71,72)*. This is consistent with the predictions from Fig. 7a which suggest that the PmrA::I13M mutant is less stable and more flexible than the wild type. Structural plasticity is an important functional feature of response regulators since it enables continuous sampling of different conformations *(73)*. Thus, this

supports the hypothesis that the introduction of a Met residue causes structural perturbations throughout the N-terminal domain, that also propagate to the C-terminal DNA-binding domain, promoting an active conformation. This could explain the increase in *pmrCAB* expression in the PmrA::I13M mutant that lead to higher colistin MICs *(24)*.

We also propose several other hypotheses for how the I13M structural changes impact PmrA's function. Since structural analysis of the well-studied response regulator Spo0F (*Bacillus subtilis*, PDB ID 1PUX) has identified a number of residues that are important for response regulator structure-function relationships, our other hypotheses predicting the effects of the PmrA::I13M mutation are based on homology of PmrA to Spo0F. The important residues identified in Spo0F include the sensor kinase and phosphatase interaction residues (Spo0F G14, I15, I17, L18, E21, and V22) *(74–76)*, the aspartyl pocket residues (Spo0F D10, D11, and D54) *(77)*, and residues surrounding the aspartyl pocket (Spo0F K104, R16, and T82) *(78)*. These correspond to PmrA residues M12, I13, E15, S16, T19 L20, D9, D10, D52, K101, A14, and S79, respectively (Fig. S3) and are discussed below. The PmrA::I13M mutation was modeled and overlaid onto the wild type I13 residue, and Fig. 7b demonstrates the orientations of some of these key residues in relation to I13.

It is predicted that residues M12, I13, S16, T19, and L20, all of which are located on the PmrA N-terminal α1 helix, likely interact with sensor kinases *(74)*. Each of these residues is in proximity of the PmrA::I13M mutation. Local structural perturbations due to the mutation would dramatically impact this whole sensor kinase interaction domain, suggesting that PmrA::I13M has altered recognition of and interactions with its cognate sensor kinase, PmrB. Since *pmrCAB* transcription was elevated in the PmrA::I13M mutant *(24)*, it is tempting to speculate that this mutation causes an altered interaction between PmrA and PmrB which promotes the active conformation of PmrA, resulting in increased DNA-binding activity. Additionally, the I13M mutation could cause relaxed kinase specificity, allowing more sensor kinases (other than

PmrB) to interact with and phosphorylate PmrA *(74,79)*. This too could explain increased DNA-binding activity of the PmrA::I13M mutant. Congruently, it is predicted that PmrA residues M12, I13, E15, and S16 are also involved in interactions with phosphatases *(75,76)*. A mutation in this region could alter interactions between PmrA and phosphatases, leading to reduced dephosphorylation, and hence increased DNA-binding. This reiterates the importance of the α1 helix for recognition by both kinases and phosphatases. Thus, it is not surprising that a single mutation such as PmrA::I13M could have a huge effect on protein-protein interactions, leading to phosphorylation-induced changes in PmrA activity.

In addition to altering interactions with sensor kinases and phosphatases, the PmrA::I13M mutation could also affect local interactions between the aspartyl pocket itself (PmrA residues D9, D10, and D52, Fig. 7b) and the surrounding residues, thus affecting the phosphorylation state. The residues surrounding the aspartyl pocket form a H-bonding network between their amino acid side chains and the phosphate oxygens. Three major residues predicted to interact with the aspartyl-phosphate (PmrA D52) are PmrA K101, A14, and S79 (Fig. 7b) *(78)*. PmrA K101 is an invariant residue at the end of the β5 sheet that is required for proper phosphorylation of response regulators and subsequent conformational changes *(63,78)*. PmrA I13 is in close proximity to K101 (Fig. 7b). Therefore, we surmise that an I13M mutation would alter this interaction and could bring K101 closer to the aspartyl pocket, stabilizing its interaction with the aspartyl phosphate. Similarly, since PmrA A14 is next to the I13M mutation (Fig. 7b), local perturbations would alter the positioning of A14, also leading to altered interactions with the aspartyl-phosphate. Although the data in Fig. 7a suggest that the PmrA::I13M mutant is more flexible overall, this is a global prediction of whole protein stability and small-scale, local stabilizations are also possible.

Phosphorylation of the aspartyl pocket also causes additional structural changes away from the site of phosphorylation via intra-protein communication networks *(78)*. Response

regulators have two highly conserved “switch” residues, PmrA Y98 and S79, that are flipped during activation to allow reorientation and interaction with the aspartyl-phosphate *(63,66)*. Therefore, these conserved residues are required for phosphorylation-induced conformational changes *(63)*. PmrA K101 is proximal to the “switch” residue, S79 (Fig. 7b). We suggest that the altered interaction between I13M, K101, and S79 could also bring S79 closer into proximity of the aspartyl pocket, further promoting this active interaction. This agrees with our data showing that PmrA::I13M-BeF_3^- binds to DNA with a tighter affinity than wt PmrA-BeF_3^- (Fig. 2d and 2c, respectively).

Intra-protein communication networks in two-domain response regulators are also vital in relaying phospho-activation signals from the N-terminal receiver domain to the C-terminal DNA-binding domain, so that it can bind DNA *(55,78)*. By analogy to Spo0F, the PmrA residues M12, I13, A14 (α1 helix), S79, Y98 (switch residues), and K101 that surround the phosphorylation site (aspartyl pocket D9, D10, D52) propagate information concerning the phosphorylation state. Such conformational changes are transmitted throughout the protein via buried residues L51 and L64 to the C-terminal end of the α3 helix, particularly R86 (Fig. 8). This region appears to be an integral part of the interface between the receiver and DNA-binding domain, with ~70% of response regulators having a Lys or Arg in this position. It is suggested that this highly conserved residue may be involved in limiting the movement of the C-terminal domain when the protein is unphosphorylated *(78)*. Interactions between R68 and the C-terminal domain can be perturbed upon activation such that the C-terminal domain is released, enabling increased conformation sampling to provide more opportunities for DNA-binding. Consequently, we hypothesize that the PmrA::I13M mutation can affect the concerted motions and conformations of the aforementioned residues in the intra-protein communication network, increasing the ability of PmrA to bind DNA, and therefore promoting colistin resistance.

To summarize, we predict that the PmrA::I13M mutation alters interactions with PmrB via the recognition face, enhances phosphorylation state, and alters the overall structure and plasticity of PmrA to promote an active conformation and therefore DNA binding. This explains the increased *pmrCAB* transcription reported previously in the PmrA::I13M strain *(24)*, and demonstrates how a single nucleotide mutation can dramatically alter protein structure and function, leading to antimicrobial resistance. An additional possibility is that the PmrA::I13M mutation affects interactions with RNA polymerase, and this too could contribute to altered transcription of the *pmrCAB* operon *(80)*.

The PmrA::P102R mutation can affect multiple components of the PmrA N-terminal domain activation mechanism

Interestingly, multiple studies have additionally reported mutations in the *A. baumannii* PmrA residue P102 (P102R *(24)*, P102H *(18)*), and also in other residues near this location (F105L *(69)*). The PmrA::P102R and PmrA::P102H mutations occurred after successive passaging of *A. baumannii* in increasing colistin concentrations *(18,24)*, whereas the strain containing the PmrA::F105L mutation was isolated from a patient receiving colistin treatment *(69)*. This suggests that this particular region of PmrA, in addition to the region around residue I13, is also susceptible to mutagenesis that promotes pathogenicity, especially in response to colistin selective pressure.

PmrA residue P102 is in the cis conformation and is located in the PmrA N-terminal domain β5-α5 loop. Although this is a somewhat unusual structural feature, this cis-Pro has been observed among many response regulators *(63)*. Pro residues contain a pyrrolidine ring which covalently binds to the backbone and restricts the conformational freedom of this amino acid *(81,82)*. This restriction means that Pro residues are often found in tight turns and loops in protein structures, as is the case in PmrA *(81)*.

We calculated the structural stability of PmrA::P102R, as we did for PmrA::I13M (Fig 7a). The restrictive nature of the pyrrolidine ring in Pro residues decreases the conformational entropy for the unfolded state. Consequently, Pro residues such as P102 can help stabilize protein structures *(83)*. Therefore, we hypothesized that the P102R mutation would decrease the stability of PmrA. Additionally, Arg residues benefit from conformational flexibility due to their long side chains *(84)* and studies show that Arg residues are less rigid than Pro residues *(85)*. This further supports our hypothesis that the PmrA::P102R structure is more flexible than wt PmrA. Simulations of PmrA::P102R predict that this mutated protein has a ΔΔG value of 0.41 kcal/mol when compared to the PmrAN structure, and ΔΔG = 1.05 kcal/mol when compared to the PmrA full-length model (Fig. 7a). Since these values are > 0 kcal/mol, these data confirm our hypothesis, indicating a reduction in protein stability and an increase in general flexibility in the PmrA::P102R mutant.

Limited conformations of P102 induced by the pyrrolidine ring also causes steric hindrance of preceding residues, such as K101 (Fig. 7c) *(86)*. Hence, the PmrA::P102R mutation would remove the cis-peptide bond to K101, relieving the conformational restraints caused by the pyrrolidine ring. This dynamic freedom would alter interactions between K101 and the aspartyl-phosphate, D52, and it is conceivable that these structural changes would promote phosphorylation and activation. This could explain the increased *pmrCAB* transcription reported in the PmrA::P102R mutant strain *(24)*.

Since the PmrA::P102R mutation perturbs the conserved K101 residue, this would also affect the S79 “switch” residue, as described above for PmrA::I13M. Alterations to S79 (Fig. 7c) may shift the equilibrium to increase sampling of the activated “switched” conformation, promoting DNA-binding *(66)*. Further supporting this, the Y98 “switch” residue is located near the P102 residue. The introduction of an Arg residue would perturb the backbone through to residue Y98, and this relaxation could allow Y98 to move more freely into the active

conformation. This provides another possible reason for increased colistin resistance in the PmrA::P102R strain.

As mentioned, P102R is located on the β5-α5 loop which forms part of the conserved α4-β5-α5 dimer interface *(61)*. Models of other response regulator dimer interaction domains allowed us to hypothesize that residue P102 is directly involved in forming the hydrophobic interface between two PmrA monomers *(68,87)*. The specific P102R mutation exchanges a hydrophobic residue for a hydrophilic one. Hydrophilic residues such as Arg are usually surface exposed and form hydrogen bonds with water molecules, whereas hydrophobic residues such as Pro are typically less exposed *(84)*. Hence, altered interactions between the exposed positive Arg and a negative residue on the partnering monomer would contribute to the network of salt bridges at the dimer interface *(61)*. This could alter the affinity between two monomers, promoting dimerization, and further confirming that the P102R mutation would enhance the DNA-binding activity of PmrA.

Furthermore, it is likely that the location of residue P102 is also accessible to sensor kinases prior to dimerization *(88,89)*. Similar to the PmrA::I13M mutation, this suggests that the PmrA::P102R mutation could affect the interaction between PmrA and PmrB. For instance, the affinity of the PmrA/PmrB interaction could increase, leading to enhanced phosphorylation. Additionally, the mutation could alter sensor kinase specificity, especially due to the flexible nature of Arg residues, leading to more interactions and phosphorylation events. Both of these occurrences would cause increased transcription of *pmrCAB* in the PmrA::P102R mutant.

Overall, we predict that PmrA::P102R impacts the N-terminal domain by altering the orientation of key residues (K101, S79, Y98) and by affecting interactions at both the dimer interface and the sensor kinase interface. Therefore, P102R affects multiple components of the activation mechanism that will have downstream structural perturbations throughout the N- and C-terminal domains. Flexibility is an essential feature of response regulators to allow sampling

of multiple conformations for DNA binding *(56)*, thus showing the potential pathogenic advantages of mutations such as P102R. Furthermore, this mutation could also alter binding to RNA polymerase, as mentioned for PmrA::I13M.

To summarize, we have predicted the *A. baumannii* PmrA consensus box as 5′-HTTAAD N_5 HTTAAD. From this, we were able to identify numerous genes in the putative PmrA regulon, including its own *pmrCAB* promoter. We have solved the structure for the *A. baumannii* PmrA N-terminal domain using X-ray crystallography and have provided a model for the full-length PmrA structure from this multidrug-resistant pathogen. Lastly, we investigated two biologically relevant PmrA mutants through biochemical and computational approaches and have provided a detailed discussion on their potential structural perturbations. These structural changes could alter PmrA function, leading to colistin resistance among *A. baumannii* clinical isolates.

FUNDING

This work was supported by the National Institutes of Health [R01 5R01AI136904-02, R01 AI136904].

ACKNOWLEDGEMENTS

Crystallographic data were collected at General Medical Sciences and Cancer Institute's Structural Biology Facility (GM/CA) 23-ID at the Advanced Photon Source, Argonne National Laboratory. We would like to thank J. Hyatt and F. Jaimes for their assistance with protein purification. We would also like to thank A. J. Milton for reviewing the manuscript.

CONFLICT OF INTEREST

None declared.

ACCESSION NUMBERS

The structure of PmrAN has been deposited to the Protein Data Bank with PDB entry ID 7M0S.

AUTHOR CONTRIBUTIONS

All authors conceived the study. S.P. and M.E.M. designed the experimental approaches. S.P. performed experiments and M.E.M. assisted S.P. with X-ray data collection and structure solving. M.E.M. performed computational work. All authors contributed to the writing of the manuscript.

REFERENCES

1. Almasaudi S.B. (2018). Acinetobacter spp. as nosocomial pathogens: Epidemiology and resistance features. *Saudi J Biol Sci*. 25(3):586–96.

2. Ayobami O., Willrich N., Harder T., Okeke I.N., Eckmanns T., and Markwart R. (2019). The incidence and prevalence of hospital-acquired (carbapenem-resistant) Acinetobacter baumannii in Europe, Eastern Mediterranean and Africa: a systematic review and meta-analysis. *Emerg Microbes Infect*. 8(1):1747–59.

3. Howard A., O'Donoghue M., Feeney A., and Sleator R.D. (2012). Acinetobacter baumannii: an emerging opportunistic pathogen. *Virulence*. 3(3):243–50.

4. Morris F.C., Dexter C., Kostoulias X., Uddin M.I., and Peleg A.Y. (2019). The Mechanisms of Disease Caused by Acinetobacter baumannii. *Front Microbiol*. 10:1601.

5. Sherertz R.J., and Sullivan M.L. (1985). An outbreak of infections with acinetobacter calcoaceticus in burn patients: Contamination of patients' mattresses. *J Infect Dis*. 151(2):252–8.

6. Wang S.H., Sheng W.H., Chang Y.Y., Wang L.H., Lin H.C., Chen M.L., et al. (2003). Healthcare-associated outbreak due to pan-drug resistant Acinetobacter baumannii in a surgical intensive care unit. *J Hosp Infect*. 53(2):97–102.

7. Fournier P.E., Richet H., and Weinstein R.A. (2006). The Epidemiology and Control of Acinetobacter baumannii in Health Care Facilities. *Clin Infect Dis*. 42(5):692–9.

8. Farrow III J.M., Wells G., and Pesci E.C. (2018). Desiccation tolerance in Acinetobacter baumannii is mediated by the two-component response regulator BfmR. *PLoS One*. 13(10).

9. Wong D., Nielsen T.B., Bonomo R.A., Pantapalangkoor P., Luna B., and Spellberg B.

(2017). Clinical and Pathophysiological Overview of Acinetobacter Infections: a Century of Challenges. *Clin Microbiol Rev*. 30(1):409–47.

10. Centers for Disease Control and Prevention (U.S.) ; National Center for Emerging Zoonotic and Infectious Diseases (U.S.). Division of Healthcare Quality Promotion. Antibiotic Resistance Coordination and Strategy Unit. (2019). Antibiotic resistance threats in the United States, 2019 [Internet]. Atlanta, GA: http://dx.doi.org/10.15620/cdc:82532; 2019.

11. Scott P.T., Petersen K., Fishbain J., Craft D.W., Ewell A.J., Moran K., et al. (2004). Morbidity and Mortality Weekly Report. 2004.

12. Matthaiou D.K., Michalopoulos A., Rafailidis P.I., Karageorgopoulos D.E., Papaioannou V., Ntani G., et al. (2008). Risk factors associated with the isolation of colistin-resistant gram-negative bacteria: a matched case-control study. *Crit Care Med*. 36(3):807–11.

13. Taccone F.S., Rodriguez-Villalobos H., De Backer D., De Moor V., Deviere J., Vincent J.-L., et al. (2006). Successful treatment of septic shock due to pan-resistant Acinetobacter baumannii using combined antimicrobial therapy including tigecycline. *Eur J Clin Microbiol Infect Dis Off Publ Eur Soc Clin Microbiol*. 25(4):257–60.

14. Park Y.K., Choi J.Y., Shin D., and Ko K.S. (2011). Correlation between overexpression and amino acid substitution of the PmrAB locus and colistin resistance in Acinetobacter baumannii. *Int J Antimicrob Agents*. 37(6):525–30.

15. Wiese A., Gutsmann T., and Seydel U. (2003). Towards antibacterial strategies: studies on the mechanisms of interaction between antibacterial peptides and model membranes. *J Endotoxin Res*. 9(2):67–84.

16. Queenan A.M., Pillar C.M., Deane J., Sahm D.F., Lynch A.S., Flamm R.K., et al. (2012).

Multidrug resistance among Acinetobacter spp. in the USA and activity profile of key agents: results from CAPITAL Surveillance 2010. *Diagn Microbiol Infect Dis*. 73(3):267–70.

17. El-Sayed Ahmed M.A.E.-G., Zhong L.-L., Shen C., Yang Y., Doi Y., and Tian G.-B. (2020). Colistin and its role in the Era of antibiotic resistance: an extended review (2000-2019). *Emerg Microbes Infect*. 9(1):868–85.

18. Adams M.D., Nickel G.C., Bajaksouzian S., Lavender H., Murthy A.R., Jacobs M.R., et al. (2009). Resistance to colistin in Acinetobacter baumannii associated with mutations in the PmrAB two-component system. *Antimicrob Agents Chemother*. 53(9):3628–34.

19. Moffatt J.H., Harper M., Harrison P., Hale J.D.F., Vinogradov E., Seemann T., et al. (2010). Colistin resistance in Acinetobacter baumannii is mediated by complete loss of lipopolysaccharide production. *Antimicrob Agents Chemother*. 54(12):4971–7.

20. Lesho E., Yoon E.-J., McGann P., Snesrud E., Kwak Y., Milillo M., et al. (2013). Emergence of Colistin-Resistance in Extremely Drug-Resistant Acinetobacter baumannii Containing a Novel pmrCAB Operon During Colistin Therapy of Wound Infections. *J Infect Dis*. 208(7):1142–51.

21. Cheah S.-E., Johnson M.D., Zhu Y., Tsuji B.T., Forrest A., Bulitta J.B., et al. (2016). Polymyxin Resistance in Acinetobacter baumannii: Genetic Mutations and Transcriptomic Changes in Response to Clinically Relevant Dosage Regimens. *Sci Rep*. 6:26233.

22. Wright M.S., Jacobs M.R., Bonomo R.A., and Adams M.D. (2017). Transcriptome Remodeling of Acinetobacter baumannii during Infection and Treatment. *MBio*. 8(2):e02193-16.

23. Trebosc V., Gartenmann S., Tötzl M., Lucchini V., Schellhorn B., Pieren M., et al. (2019).

Dissecting Colistin Resistance Mechanisms in Extensively Drug-Resistant Acinetobacter baumannii Clinical Isolates. *MBio*. 10(4).

24. Sun B., Liu H., Jiang Y., Shao L., Yang S., and Chen D. (2020). New Mutations Involved in Colistin Resistance in Acinetobacter baumannii. *mSphere*. 5(2):e00895-19.

25. Huang J., Li C., Song J., Velkov T., Wang L., Zhu Y., et al. (2020). Regulating polymyxin resistance in Gram-negative bacteria: roles of two-component systems PhoPQ and PmrAB. *Future Microbiol*. 15(6):445–59.

26. Mmatli M., Mbelle N.M., Maningi N.E., and Osei Sekyere J. (2020). Emerging Transcriptional and Genomic Mechanisms Mediating Carbapenem and Polymyxin Resistance in Enterobacteriaceae: a Systematic Review of Current Reports. *mSystems*. 5(6):e00783-20.

27. Gunn J.S. (2008). The Salmonella PmrAB regulon: lipopolysaccharide modifications, antimicrobial peptide resistance and more. *Trends Microbiol*. 16(6):284–90.

28. Wösten M.M., and Groisman E.A. (1999). Molecular characterization of the PmrA regulon. *J Biol Chem*. 274(38):27185–90.

29. Wright M.S., Iovleva A., Jacobs M.R., Bonomo R.A., and Adams M.D. (2016). Genome dynamics of multidrug-resistant Acinetobacter baumannii during infection and treatment. *Genome Med*. 8(1):26.

30. Bourret R.B., and Silversmith R.E. (2010). Two-component signal transduction. *Curr Opin Microbiol*. 13(2):113–5.

31. Desai S.K., and Kenney L.J. (2017). To ~P or Not to ~P? Non-canonical activation by two-component response regulators. *Mol Microbiol*. 103(2):203–13.

32. Draughn G.L., Milton M.E., Feldmann E.A., Bobay B.G., Roth B.M., Olson A.L., et al.

(2018). The Structure of the Biofilm-controlling Response Regulator BfmR from Acinetobacter baumannii Reveals Details of Its DNA-binding Mechanism. *J Mol Biol*. 430(6):806–21.

33. Bachhawat P., Swapna G.V.T., Montelione G.T., and Stock A.M. (2005). Mechanism of activation for transcription factor PhoB suggested by different modes of dimerization in the inactive and active states. *Structure*. 13(9):1353–63.

34. Cho H., Wang W., Kim R., Yokota H., Damo S., Kim S.H., et al. (2001). BeF(3)(-) acts as a phosphate analog in proteins phosphorylated on aspartate: structure of a BeF(3)(-) complex with phosphoserine phosphatase. *Proc Natl Acad Sci U S A*. 98(15):8525–30.

35. Otwinowski Z., and Minor W. (1997). [20] Processing of X-ray diffraction data collected in oscillation mode. In: Methods in Enzymology. New York: Academic Press; 1997. p. 307–26.

36. Liebschner D., Afonine P. V, Baker M.L., Bunkóczi G., Chen V.B., Croll T.I., et al. (2019). Macromolecular structure determination using X-rays, neutrons and electrons: recent developments in Phenix. *Acta Crystallogr Sect D, Struct Biol*. 75(Pt 10):861–77.

37. Dean S.N., Milton M.E., Cavanagh J., and van Hoek M.L. (2020). Francisella novicida Two-Component System Response Regulator BfpR Modulates iglC Gene Expression, Antimicrobial Peptide Resistance, and Biofilm Production. *Front Cell Infect Microbiol*. 10:82.

38. Emsley P., Lohkamp B., Scott W.G., and Cowtan K. (2010). Features and development of Coot. *Acta Crystallogr D Biol Crystallogr*. 66(Pt 4):486–501.

39. Schrodinger L. (2010). The PyMOL Molecular Graphics System. 2010. p. Version 1.3r1.

40. Eswar N., Webb B., Marti-Renom M.A., Madhusudhan M.S., Eramian D., Shen M.-Y., et

al. (2006). Comparative protein structure modeling using Modeller. *Curr Protoc Bioinforma*. Chapter 5:Unit-5.6.

41. Menon S., and Wang S. (2011). Structure of the response regulator PhoP from Mycobacterium tuberculosis reveals a dimer through the receiver domain. *Biochemistry*. 50(26):5948–57.

42. Lou Y.-C., Weng T.-H., Li Y.-C., Kao Y.-F., Lin W.-F., Peng H.-L., et al. (2015). Structure and dynamics of polymyxin-resistance-associated response regulator PmrA in complex with promoter DNA. *Nat Commun*. 6(1):8838.

43. Narayanan A., Kumar S., Evrard A.N., Paul L.N., and Yernool D.A. (2014). An asymmetric heterodomain interface stabilizes a response regulator–DNA complex. *Nat Commun*. 5(1):3282.

44. Milton M.E., Allen C.L., Feldmann E.A., Bobay B.G., Jung D.K., Stephens M.D., et al. (2017). Structure of the Francisella response regulator QseB receiver domain, and characterization of QseB inhibition by antibiofilm 2-aminoimidazole-based compounds. *Mol Microbiol*. 106(2):223–35.

45. (2010). PROCHECK and PROCHECK-NMR [Internet]. 2010.

46. Bhattacharya A., Tejero R., and Montelione G.T. (2007). Evaluating protein structures determined by structural genomics consortia. *Proteins*. 66(4):778–95.

47. Baek M., DiMaio F., Anishchenko I., Dauparas J., Ovchinnikov S., Lee G.R., et al. (2021). Accurate prediction of protein structures and interactions using a 3-track network. *Science (80-)*. 373(6557):871–6.

48. Hamidian M., Wick R.R., Hartstein R.M., Judd L.M., Holt K.E., and Hall R.M. (2019). Insights from the revised complete genome sequences of Acinetobacter baumannii

strains AB307-0294 and ACICU belonging to global clones 1 and 2. *Microb genomics*. 5(10).

49. Cheng H.-Y., Chen Y.-F., and Peng H.-L. (2010). Molecular characterization of the PhoPQ-PmrD-PmrAB mediated pathway regulating polymyxin B resistance in Klebsiella pneumoniae CG43. *J Biomed Sci*. 17(1):60.

50. Lou Y.-C., Wang I., Rajasekaran M., Kao Y.-F., Ho M.-R., Hsu S.-T.D., et al. (2014). Solution structure and tandem DNA recognition of the C-terminal effector domain of PmrA from Klebsiella pneumoniae. *Nucleic Acids Res*. 42(6):4080–93.

51. Kuzmic P. (1996). Program DYNAFIT for the analysis of enzyme kinetic data: application to HIV proteinase. *Anal Biochem*. 237(2):260–73.

52. Gasteiger E., Gattiker A., Hoogland C., Ivanyi I., Appel R.D., and Bairoch A. (2003). ExPASy: The proteomics server for in-depth protein knowledge and analysis. *Nucleic Acids Res*. 31(13):3784–8.

53. Khosa S., Hoeppner A., Gohlke H., Schmitt L., and Smits S.H.J. (2016). Structure of the Response Regulator NsrR from Streptococcus agalactiae, Which Is Involved in Lantibiotic Resistance. *PLoS One*. 11(3):e0149903.

54. Gao R., and Stock A.M. (2010). Molecular strategies for phosphorylation-mediated regulation of response regulator activity. *Curr Opin Microbiol*. 13(2):160–7.

55. Feher V.A., and Cavanagh J. (1999). Millisecond-timescale motions contribute to the function of the bacterial response regulator protein Spo0F. *Nature*. 400(6741):289–93.

56. Milton M.E., Minrovic B.M., Harris D.L., Kang B., Jung D., Lewis C.P., et al. (2018). Re-sensitizing Multidrug Resistant Bacteria to Antibiotics by Targeting Bacterial Response Regulators: Characterization and Comparison of Interactions between 2-Aminoimidazoles

and the Response Regulators BfmR from Acinetobacter baumannii and QseB from Fr. *Front Mol Biosci*. 5(15).

57. Goulian M. (2010). Two-component signaling circuit structure and properties. *Curr Opin Microbiol*. 13(2):184–9.

58. Raetz C.R., and Newman K.F. (1979). Diglyceride kinase mutants of Escherichia coli: inner membrane association of 1,2-diglyceride and its relation to synthesis of membrane-derived oligosaccharides. *J Bacteriol*. 137(2):860–8.

59. Cote J.M., and Taylor E.A. (2017). The Glycosyltransferases of LPS Core: A Review of Four Heptosyltransferase Enzymes in Context. *Int J Mol Sci*. 18(11):2256.

60. Wang X., Preston J.F. 3rd, and Romeo T. (2004). The pgaABCD locus of Escherichia coli promotes the synthesis of a polysaccharide adhesin required for biofilm formation. *J Bacteriol*. 186(9):2724–34.

61. Toro-Roman A., Wu T., and Stock A.M. (2005). A common dimerization interface in bacterial response regulators KdpE and TorR. *Protein Sci*. 14(12):3077–88.

62. Volz K. (1993). Structural conservation in the CheY superfamily. *Biochemistry*. 32(44):11741–53.

63. Bourret R.B. (2010). Receiver domain structure and function in response regulator proteins. *Curr Opin Microbiol*. 13(2):142–9.

64. Bachhawat P., and Stock A.M. (2007). Crystal Structures of the Receiver Domain of the Response Regulator PhoP from Escherichia coli in the Absence and Presence of the Phosphoryl Analog Beryllofluoride. *J Bacteriol*. 189(16):5987 LP – 5995.

65. Toro-Roman A., Mack T.R., and Stock A.M. (2005). Structural analysis and solution studies of the activated regulatory domain of the response regulator ArcA: a symmetric

dimer mediated by the alpha4-beta5-alpha5 face. *J Mol Biol*. 349(1):11–26.

66. Stock A.M., and Guhaniyogi J. (2006). A new perspective on response regulator activation. *J Bacteriol*. 188(21):7328–30.

67. Ouyang Z., Zheng F., Chew J.Y., Pei Y., Zhou J., Wen K., et al. (2019). Deciphering the activation and recognition mechanisms of Staphylococcus aureus response regulator ArlR. *Nucleic Acids Res*. 47(21):11418–29.

68. Qing X.-Y., Steenackers H., Venken T., De Maeyer M., and Voet A. (2017). Computational Studies of the Active and Inactive Regulatory Domains of Response Regulator PhoP Using Molecular Dynamics Simulations. *Mol Inform*. 36(11).

69. Mustapha M.M., Li B., Pacey M.P., Mettus R.T., McElheny C.L., Marshall C.W., et al. (2018). Phylogenomics of colistin-susceptible and resistant XDR Acinetobacter baumannii. *J Antimicrob Chemother*. 73(11):2952–9.

70. Arroyo L.A., Herrera C.M., Fernandez L., Hankins J. V, Trent M.S., and Hancock R.E.W. (2011). The pmrCAB operon mediates polymyxin resistance in Acinetobacter baumannii ATCC 17978 and clinical isolates through phosphoethanolamine modification of lipid A. *Antimicrob Agents Chemother*. 55(8):3743–51.

71. Gellman S.H. (1991). On the role of methionine residues in the sequence-independent recognition of nonpolar protein surfaces. *Biochemistry*. 30(27):6633–6.

72. Aledo J.C. (2019). Methionine in proteins: The Cinderella of the proteinogenic amino acids. *Protein Sci*. 28(10):1785–96.

73. McEvoy M.M., Hausrath A.C., Randolph G.B., Remington S.J., and Dahlquist F.W. (1998). Two binding modes reveal flexibility in kinase/response regulator interactions in the bacterial chemotaxis pathway. *Proc Natl Acad Sci U S A*. 95(13):7333–8.

74. Szurmant H., Bobay B.G., White R.A., Sullivan D.M., Thompson R.J., Hwa T., et al. (2008). Co-evolving motions at protein-protein interfaces of two-component signaling systems identified by covariance analysis. *Biochemistry*. 47(30):7782–4.

75. Tzeng Y.L., Feher V.A., Cavanagh J., Perego M., and Hoch J.A. (1998). Characterization of interactions between a two-component response regulator, Spo0F, and its phosphatase, RapB. *Biochemistry*. 37(47):16538–45.

76. McLaughlin P.D., Bobay B.G., Regel E.J., Thompson R.J., Hoch J.A., and Cavanagh J. (2007). Predominantly buried residues in the response regulator Spo0F influence specific sensor kinase recognition. *FEBS Lett*. 581(7):1425–9.

77. Tzeng Y.-L., and Hoch J.A. (1997). Molecular recognition in signal transduction: the interaction surfaces of the Spo0F response regulator with its cognate phosphorelay proteins revealed by alanine scanning mutagenesis. *J Mol Biol*. 272(2):200–12.

78. Feher V.A., Tzeng Y.L., Hoch J.A., and Cavanagh J. (1998). Identification of communication networks in Spo0F: a model for phosphorylation-induced conformational change and implications for activation of multiple domain bacterial response regulators. *FEBS Lett*. 425(1):1–6.

79. Jiang M., Tzeng Y.L., Feher V.A., Perego M., and Hoch J.A. (1999). Alanine mutants of the Spo0F response regulator modifying specificity for sensor kinases in sporulation initiation. *Mol Microbiol*. 33(2):389–95.

80. Blanco A.G., Canals A., Bernués J., Solà M., and Coll M. (2011). The structure of a transcription activation subcomplex reveals how σ(70) is recruited to PhoB promoters. *EMBO J*. 30(18):3776–85.

81. MacArthur M.W., and Thornton J.M. (1991). Influence of proline residues on protein

conformation. *J Mol Biol*. 218(2):397–412.

82. Ho B.K., and Brasseur R. (2005). The Ramachandran plots of glycine and pre-proline. *BMC Struct Biol*. 5(1):14.

83. Choi E.J., and Mayo S.L. (2006). Generation and analysis of proline mutants in protein G. *Protein Eng Des Sel*. 19(6):285–9.

84. Shalit Y., and Tuvi-Arad I. (2020). Side chain flexibility and the symmetry of protein homodimers. *PLoS One*. 15(7):e0235863–e0235863.

85. Huang F., and Nau W.M. (2003). A conformational flexibility scale for amino acids in peptides. *Angew Chem Int Ed Engl*. 42(20):2269–72.

86. Schimmel P.R., and Flory P.J. (1968). Conformational energies and configurational statistics of copolypeptides containing L-proline. *J Mol Biol*. 34(1):105–20.

87. Solà M., Gomis-Rüth F.X., Serrano L., González A., and Coll M. (1999). Three-dimensional crystal structure of the transcription factor PhoB receiver domain. *J Mol Biol*. 285(2):675–87.

88. Xie M., Wu M., and Han A. (2020). Structural insights into the signal transduction mechanism of the K+-sensing two-component system KdpDE. *Sci Signal*. 13(643):eaaz2970.

89. Zapf J., Sen U., Madhusudan, Hoch J.A., and Varughese K.I. (2000). A transient interaction between two phosphorelay proteins trapped in a crystal lattice reveals the mechanism of molecular recognition and phosphotransfer in signal transduction. *Structure*. 8(8):851–62.

Figure 1. Defining the *A. baumannii* PmrA binding motif. (a) KpPmrA_25mer DNA sequence derived from the *K. pneumoniae* PmrA box *(42)*. Inverted repeat sequences are underlined. **(b)** EMSAs showing binding of wt PmrA, PmrA::I13M, and wt PmrA-BeF_3^- to 1 µM KpPmrA_25mer. Arrows indicate positions of mobility shifts.

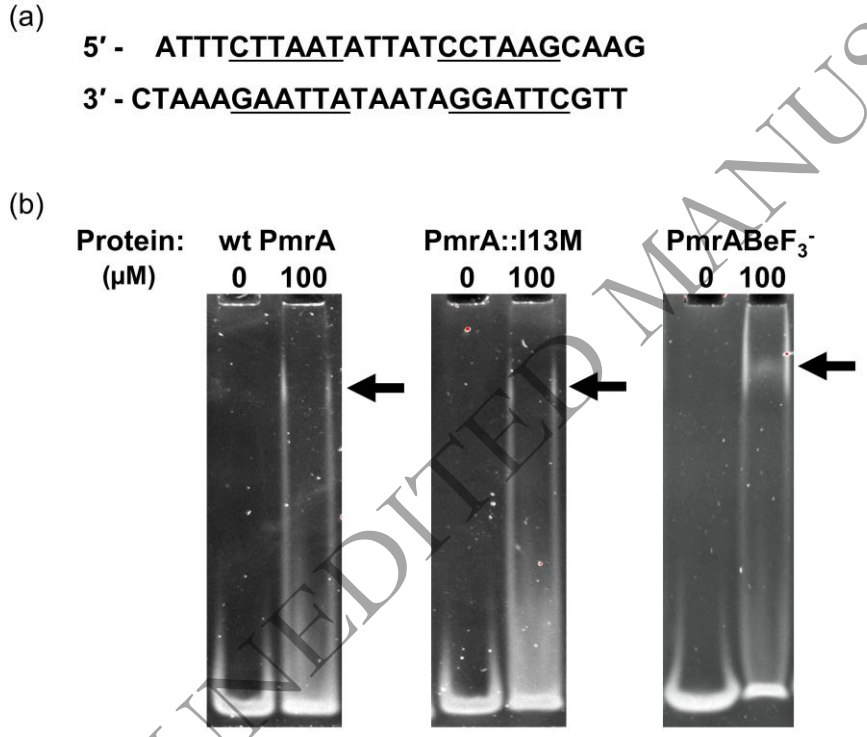

Figure 2. DNA binding affinities of *A. baumannii* PmrA. DNA fluorescent anisotropy was used to determine the DNA binding affinities of wt PmrA **(a)**, PmrA::I13M **(b)**, wt PmrA-BeF_3^- **(c)**, and PmrA::I13M-BeF_3^- **(d)** binding to the KpPmrA_25mer_

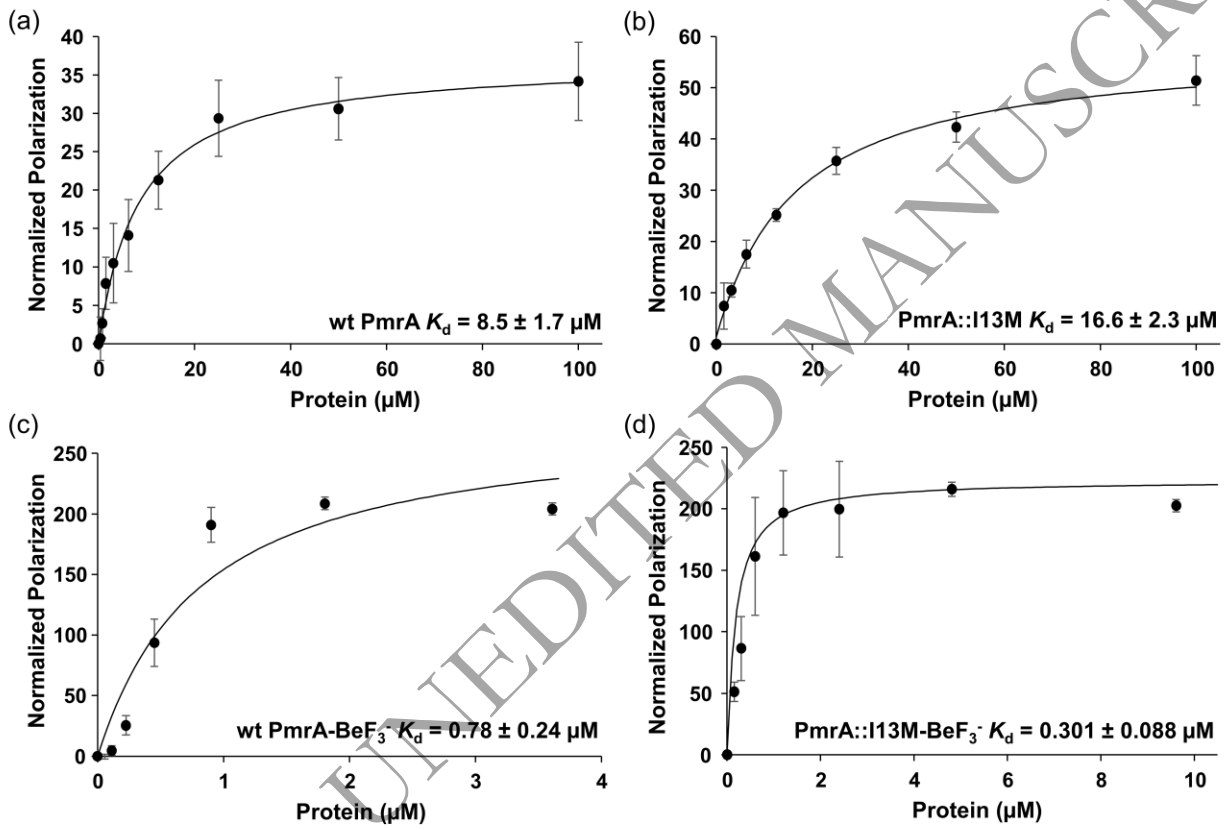

Figure 3. *A. baumannii* PmrA binds to the *pmrCAB* promoter. EMSAs showing binding of wt PmrA, PmrA::I13M and wt PmrA-BeF_3^- binding to 2 µM AbPmrC_27mer. Arrows indicate positions of mobility shifts.

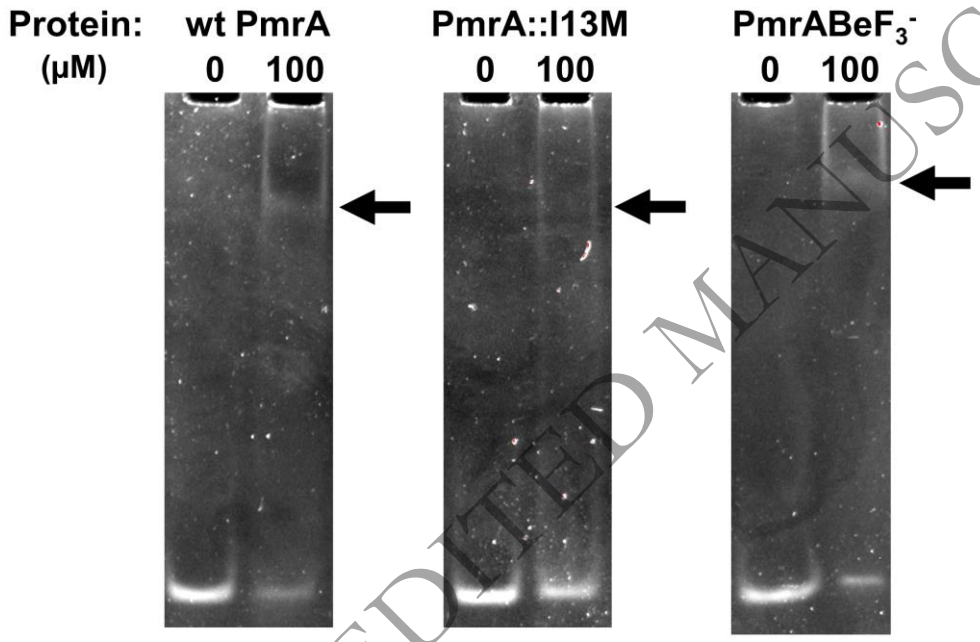

Figure 4. X-ray crystal structure of *A. baumannii* PmrAN. (a) The N-terminal domain of PmrA is a homodimer with each monomer colored individually. The structure was solved and refined to 1.64 Å. Secondary structural elements are labeled. **(b)** PmrAN Arg118 shares density between the two monomer chains, allowing two alternative conformations for each. An interacting water molecule is shown in red. H-bonds are shown in yellow.

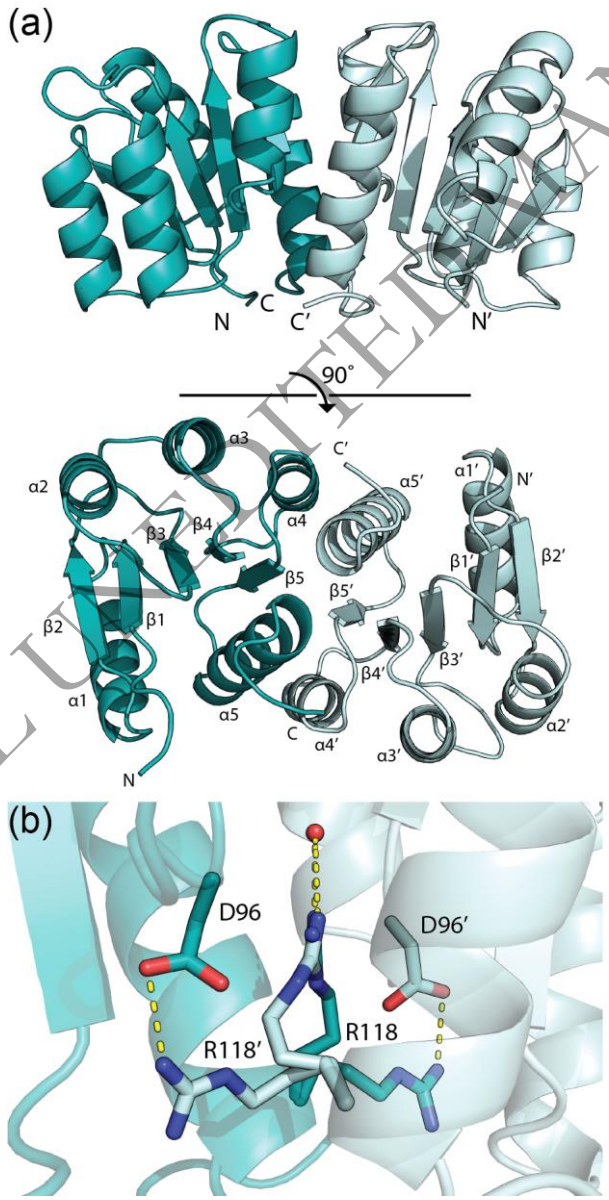

Figure 5. Structural alignment of *A. baumannii* PmrAN with other response regulators. (a) Structural alignment of our PmrAN structure to 16 other response regulator protein structures from the Protein Data Bank (PDB). *A. baumannii* PmrA is shown in teal and other response regulators are shown in grey. **(b)** Table showing RMSD values for alignment of each structure with *A. baumannii* PmrAN. A lower RMSD value indicates higher similarity between structures. Alignments were performed to chain A of each PDB structure. Values were calculated using PyMol.

(a)

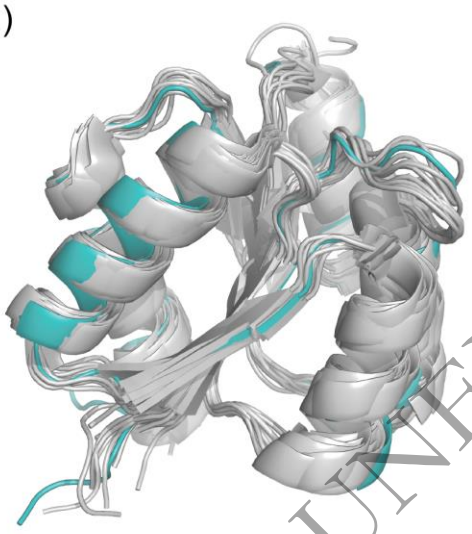

(b)

PDB ID	Protein	Organism	RMSD to PmrA (Å)
1NXX	MicA	Streptococcus pneumoniae	0.760
1YS6	PrrA	Mycobacterium tuberculosis	1.044
1ZH2	KdpE	Escherichia coli	0.934
2A9R	YycF	Streptococcus pneumoniae	0.734
2PL1	PhoP	Escherichia coli	0.880
3NNN	DrrD	Thermotoga maritima	0.992
3R0J	PhoP	Mycobacterium tuberculosis	1.078
4KFC	KdpE	Escherichia coli	0.784
4KNY	KdpE	Escherichia coli	0.760
4S04	PmrA	Klebsiella pneumoniae	0.949
4S05	PmrA	Klebsiella pneumoniae	1.077
5UIC	QseB	Francisella tularensis novicida	0.935
6BR7	BfmR	Acinetobacter baumannii	1.011
6EBR	YycF	Streptococcus pneumoniae	0.752
6IS2	ArlR	Staphylococcus aureus	0.723
6ONT	BfpR	Francisella tularensis novicida	1.160

Figure 6. Model of full-length *A. baumannii* PmrA. (a) A full-length model of PmrA was generated based on the *A. baumannii* PmrAN crystal structure (Fig. 4) in addition to other homologous structures, as listed in the Materials and Methods. **(b)** Structural alignment of our *A. baumannii* PmrA model with a RoseTTAFold structural prediction of the PmrA C-terminal domain. RoseTTAFold output the top five models. The top model (model01) has a confidence score of 0.8391 (RMSD between model01 and PmrA is 1.101 Å).

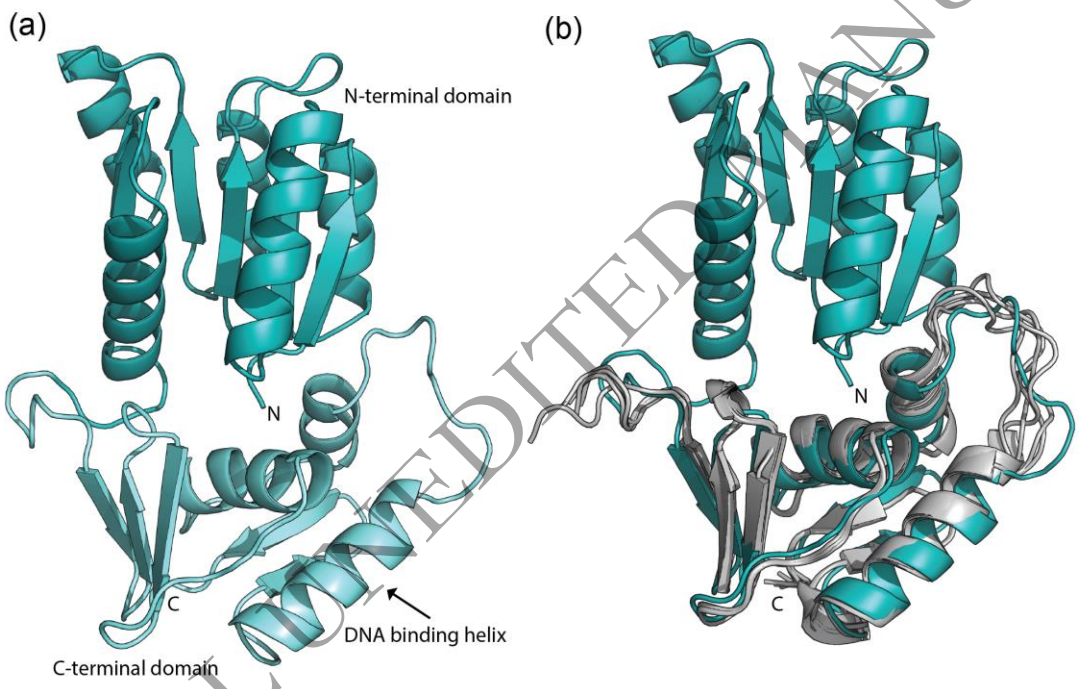

Figure 7. Simulations of biologically relevant PmrA point mutants. (a) The PmrA::I13M and PmrA::P102R mutated proteins were compared to the wild type PmrAN structure and the PmrA full-length model to predict structural stability, whereby a ΔΔG value > 0 kcal/mol is considered destabilizing. **(b)** The PmrA::I13M mutation (pink) was modeled and overlaid onto the wild type I13 residue (teal). Other relevant residues are also labeled. **(c)** The PmrA::P102R mutation (pink) was modeled and overlaid onto the wild type P102 residue (teal). Other relevant residues are also labeled.

(a)

	PmrAN		PmrA model	
Run #	I13M	P102R	I13M	P102R
1	0.49	0.41	0.11	1.35
2	0.5	0.47	0.1	1.28
3	0.57	0.27	0.57	0.75
4	0.59	0.39	0.16	0.51
5	0.48	0.44	0.13	0.99
6	0.41	0.45	0.79	1.36
7	0.51	0.45	0.67	1.36
8	0.51	0.38	0.08	1.2
9	0.53	0.41	-0.06	1.34
10	0.55	0.43	0.53	0.35
Average ΔΔG	0.51	0.41	0.31	1.05

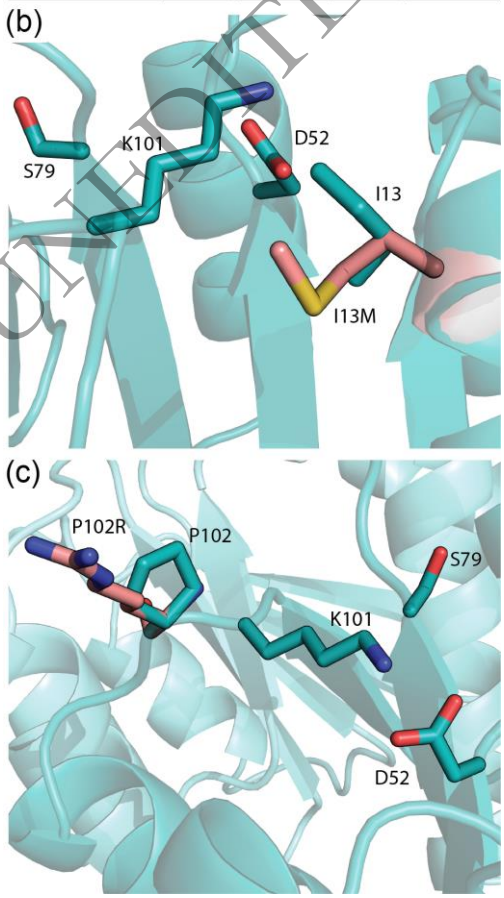

Figure 8. Intra-protein communication network. Top and side view of PmrA highlighting residues involved in intra-protein communication from the phosphorylation site to the DNA-binding domain. Aspartyl pocket residues (D9, D10, and D52) are shown in cream. Key residues surrounding the aspartyl pocket (M12, M13, A14, and K101) and switch residues (S79 and Y98) are shown in blue. Buried hydrophobic residues that transmit the signal through the protein (L51 and L64) are in purple. R68 is highlighted in orange.

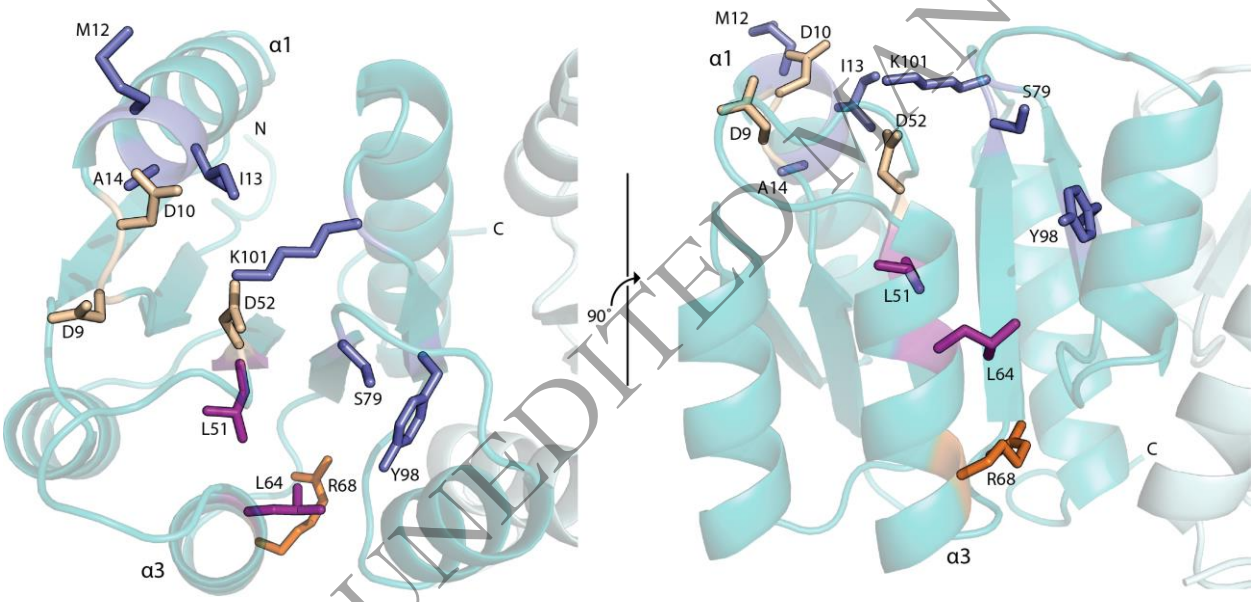

Figure S1. EMSA overlay images

Figure S2. Structural alignment of *A. baumannii* PmrAN with other response regulator dimers

Figure S3. PmrA and Spo0F alignment

Table S1. Bacterial strains and plasmids

Table S2. Oligomers

Table S3. PmrAN collection and refinement

Table I. Putative *A. baumannii* PmrA Regulon

ACICU Locus Tag[a]	Predicted Function[b]	Motif Identified (5' → 3')	Distance between Motif and TSS[c] (Bp)
ACICU_03004 – ACICU_03002	PmrC, PmrA, PmrB	**TTTAAG** N_5 **TTTAAG**	48
ACICU_03001	Putative lipid A 4'-phosphatase (LpxF-like)	**ATTAAA** N_3 **ATTAAA**	103
ACICU_01072	Putative lipid A pEtN transferase	**TTTAAT** N_6 **ATTAAT**	79
ACICU_02907	Diacylglycerol kinase	**TTTAAT** N_5 **TTTAAG** **TTTAAA** N_5 **TTTAAT**	44 55
ACICU_02865 – ACICU_02868	Hypothetical glycosyl transferase family 2	**TTTAAG** N_5 **ATTAAG** **CTTAAG** N_5 **TTTAAG**	85 96
ACICU_00900 – ACICU_00902	PgaD, PgaC, PgaB	**CTTAAG** N_0 **TTTAAA** **CTTAAG** N_5 **AATAAA** **TTTAAA** N_2 **TTTAAG**	41 67 148
ACICU_02895	Putative polyketide synthase modules	**TTTAAG** N_4 **CTTAAT** **TTTAAT** N_5 **TTTAAG**	92 102
ACICU_03041	SbmA	**TTTAAA** N_3 **ATTAAA**	227
ACICU_01552 – ACICU_01551	Hypothetical proteins	**TTTAAG** N_1 **TTTAAT** **TTTAAG** N_5 **TTTAAG**	51 58
ACICU_01518	Hypothetical protein	**CTTAAA** N_5 **ATTAAA**	126
ACICU_00741	Uncharacterized (COG3216)	**TTTAAG** N_2 **TTTAAT** **TTTAAT** N_1 **TTTAAG**	60 68

[a] Selected from transcriptome study *(22)*

[b] Referenced from ACICU genome *(48)*

[c] TSS = Translational Start Site